Journal of Materials Chemistry C

Accepted Manuscript

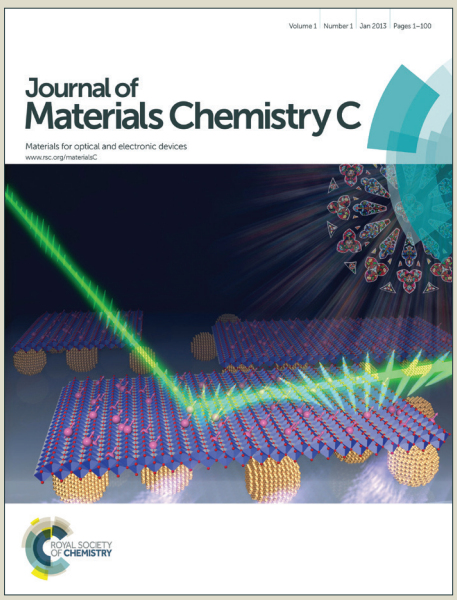

ROYAL SOCIETY OF CHEMISTRY

www.rsc.org/materialsC

Cite this: DOI: 10.1039/x0xx00000x

Transistor application of new picene-type molecules, 2,9-dialkylated phenanthro[1,2-*b*:8,7-*b*']dithiophenes

Yoshihiro Kubozono*[a,b,c], Keita Hyodo[d], Hiroki Mori[d], Shino Hamao[a], Hidenori Goto[a] and Yasushi Nishihara*[b,c,d]

Received 00th January 2012,
Accepted 00th January 2012

DOI: 10.1039/x0xx00000x

www.rsc.org/

Field-effect transistors (FETs) have been fabricated with thin films of a series of 2,9-dialkylated phenanthro[1,2-*b*:8,7-*b*']dithiophene derivatives (C_n-PDTs). The FET characteristics of C_n-PDT thin-film FETs with an SiO_2 gate dielectric as well as high-*k* gate dielectrics were recorded, and the dependence of the field-effect mobility, μ, on the number (n) of carbons in alkyl chains was investigated, showing that the 2,9-didodecylphenanthro[1,2-*b*:8,7-*b*']dithiophene (C_{12}-PDT) thin-film FET displays superior properties, with μ's as high as 1.8 $cm^2\ V^{-1}\ s^{-1}$ for the SiO_2 gate dielectric and 2.2 $cm^2\ V^{-1}\ s^{-1}$ for the HfO_2 gate dielectric. The average μ values, $<\mu>$'s, reach 1.1(5) and 1.8(6) $cm^2\ V^{-1}\ s^{-1}$, respectively, for the SiO_2 and ZrO_2 gate dielectrics. Low-voltage operation, showing an absolute average threshold voltage $<|V_{th}|>$ of ~ 11 V was implemented, together with the above high $<\mu>$ of ~ 2 $cm^2\ V^{-1}\ s^{-1}$. Also, a flexible FET was fabricated with a parylene gate dielectric. The results of this study show the potential for application of the C_{12}-PDT molecule in a high-performance transistor.

Introduction

Organic field-effect transistors (FETs) have attracted much attention as the key elements for realizing future ubiquitous electronics because of their numerous advantages, including flexibility, light weight, and ease of design.[1-4] During past 25 years, many organic materials have been used to fabricate high-performance organic thin-film FETs.[5-22] Representative organic molecules used in p-channel organic FETs are acenes,[5-13] oligomers[14-16] and tetrathiafulvalenes,[17,18] while those used in n-channel FETs are perylenediimides,[19-22] C_{60}'s[23,24] and fused thiophene-type molecules[25-27]. Among these, higher values of field-effect mobility (μ) have principally been reported in FETs using acene-type molecules.[5-13] Therefore, acene-type molecules are the most popular choices as active layers in organic FETs.

One acene-type molecule in particular, pentacene, has served as the active semiconducting layer in organic thin-film FETs owing to its high μ value of 3.0 $cm^2\ V^{-1}\ s^{-1}$,[6] and its low cost.[6] Furthermore, FETs using single crystals of various molecules[28-32] as the active layer have been extensively investigated during the past decade, displaying high μ values of more than 1 $cm^2\ V^{-1}\ s^{-1}$ because of their lack of grain boundaries and low level of defects. In particular, single crystals of rubrene have provided excellent FET characteristics, with μ as high as 40 $cm^2\ V^{-1}\ s^{-1}$.[29] At present, using thin-film pentacene or single-crystal rubrene has become the most standard process in fabricating high-performance organic FETs. Nevertheless, the pentacene molecule is not air-stable owing to its relatively high HOMO level (–5.0 eV), which originates in its extended π-conjugation.[33] The rubrene molecule has scarcely been available for thin-film FETs, *i.e.*, very few rubrene thin-film FETs have been operated.[34-38]

Recently, phenacene-type molecules (Fig. 1), which have a W-shaped structure, have attracted considerable attention in materials science and solid-state physics because the chemical doping of solid phenacene with alkali metals provided superconductivity.[39,40] Furthermore, application of phenacene molecules in transistors has shown good FET characteristics.[41-47] Very recently, thin-film FET based on new phenacene-type molecule, 3,10-ditetradecylpicene (picene-$(C_{14}H_{29})_2$),[38] showed μ value as high as 20.9 $cm^2\ V^{-1}\ s^{-1}$, which is the second highest in organic thin film FETs; the highest μ value in organic thin-film FETs is now 43 $cm^2\ V^{-1}\ s^{-1}$ achieved for 2,7-dioctyl[1]benzothieno[3,2-*b*][1]benzothiophene, C8-BTBT.[48] FETs based on thin-film phenacenes operated well even under ambient atmospheric conditions.[41-45,49,50] In particular, the thin-film FET using picene, one of the phenacene family of molecules, showed O_2 sensing properties in that the μ value increased dramatically under atmospheric conditions.[41,42,49,50] Phenacene molecules are very stable under atmospheric conditions because of their large energy band-gap (E_g = 3.3 eV) and deep HOMO level (E_{HOMO} ~ –5.5 eV)[41-45,47,51] compared with those (E_g = 1.6 eV, E_{HOMO} = –5.0 eV)[33] of pentacene. Therefore, further improvement of the FET properties is greatly desired owing to the advantages of phenacene molecules described above.

We have recently reported the synthesis of picene[52] and fulminene[53] by the palladium-catalyzed Suzuki-Miyaura coupling of (*Z*)-alkenylboronates with polyhalobenzene and sequential intramolecular double cyclization through C–H activation. This protocol is also applicable to the synthesis of

phenanthro[1,2-*b*:8,7-*b'*]dithiophene (PDT) by replacing two terminal phenyl rings in picene with thiophene rings, aiming at increased intermolecular π-π interactions due to the large atomic radius of sulfur, thereby improving the FET characteristics. FET devices fabricated with thin films of PDT formed by thermal deposition exhibited a μ as high as 1.1×10^{-1} cm^2 V^{-1} s^{-1},[54] which was lower by one order of magnitude than that (1.1 cm^2 V^{-1} s^{-1}) of the picene thin-film FET.[41,42] The next strategy for increasing μ in a PDT FET is to use dialkyl-substituted PDTs, in which two alkyl substituents (C_nH_{2n+1}) are added to the PDT molecule, *i.e.*, PDT-$(C_nH_{2n+1})_2$. This molecule is referred to as 'C_n-PDT' in this paper. This idea is based on the expectation of forming a strong intermolecular π-π stacking, which may be encouraged by the interaction of alkyl substituents in what is called the 'fastener effect'. In other words, the installation of long alkyl chains onto π-frameworks fastens the π-core of the molecule tightly through van der Waals interaction between alkyl-chains.[55] Actually, dialkyl-substituted picene (picene-$(C_{14}H_{29})_2$) provided a very high μ value, as described above.[46] The alkyl substitution of PDT may be applicable to the fabrication of solution-processed FETs, because the solubility in common organic solvents is improved. Such examples have already been reported in alkyl-substituted picene[46] and alkylated thienoacene.[8,56] Our group recently reported a useful synthetic route to C_n-PDTs (n = 7–14),[57] which is the first step towards the use of C_n-PDTs in electronics. Here, it should be noted that $InCl_3$-catalyzed cyclization reaction of the diepoxide can produce PDT as well as its isomer, anthra[1,2-*b*:5,6-*b'*]dithiophene, but that PDT used in this study is the pure form. The reason why the PDT was selectively synthesized is described in our previous paper.[57]

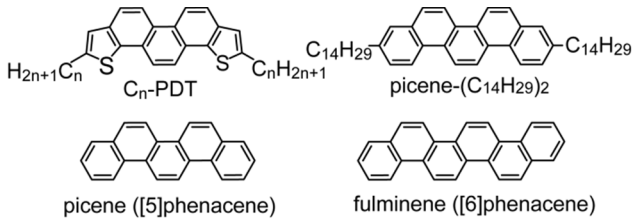

Fig. 1. Molecular structures of PDT and phenacene analogues.

In this report we evaluate the FET characteristics of C_n-PDT thin-film FETs to demonstrate the positive effect on FET performance of alkyl-substitution in PDT. In this study, the topological and electronic features of thin films of C_n-PDTs have been clarified using X-ray diffraction (XRD)/atomic force microscopy (AFM) and photoelectron yield spectroscopy (PYS)/optical absorption spectroscopy, respectively. Theoretical calculations on C_n-PDT molecules have been achieved within the framework of density functional theory (DFT). FETs based on thin films of C_n-PDTs have been fabricated using SiO_2 gate dielectrics, and the dependence of μ on the number of carbons (n) has been investigated. The highest μ value has been recorded in a C_{12}-PDT thin-film FET, and the reason why C_{12}-PDT provides such good FET characteristics is discussed based on the topological and electronic features of its thin film. Also, FETs have been fabricated with thin films of C_{12}-PDT and using high-*k* gate dielectrics. A flexible C_{12}-PDT thin-film FET has also been fabricated with a parylene gate dielectric and a polyethylene terephthalate (PET) substrate. This study is part of an exploration of potentially practical applications of phenacene analogues in electronics, such as the use of C_n-PDTs in FETs.

Experimental

All C_n-PDTs used in this study were synthesized according to our procedure described previously.[57] The XRD patterns of C_n-PDT thin films fabricated by thermal deposition were measured using Smart Lab-Pro (Rigaku), and an X-ray wavelength of 1.5418 Å (Cu Kα source). The AFM images were recorded in a tapping mode using an SPA 400-DFM (SII Nano Technologies). The PYS and optical absorption spectra were measured using a BIP-KV201AD photoelectron yield measurement system and a SHIMADZU UV-2450 absorption spectrometer, respectively. The DFT calculations were performed at the B3LYP/6-31G(d) level using the Gaussian 09, Revision A.02 program package.[58-61]

FET devices using thin films (60 nm) of C_n-PDTs were fabricated on SiO_2 (400 nm)/Si, HfO_2 (50 nm)/Si, Ta_2O_5 (50 nm)/Si, ZrO_2 (50 nm)/Si, $PbZr_{0.52}Ti_{0.48}O_3$ (PZT: 150 nm)/Si, and parylene (1000 nm)/PET substrates by thermal deposition in a home-made vacuum chamber. The growth condition of thin films was the same for all thin films of C_n-PDTs; deposition rate was 0.5 Å / s and the substrate temperature was kept at room temperature. Namely, in this paper, we did not pursue the difference of film's properties which may be caused by the difference under growth conditions. The base pressure was maintained below 10^{-7} Torr. The SiO_2 surface was treated with hexamethyldisilazane (HMDS) to produce a hydrophobic surface. The surface of the high-*k* gate dielectrics (HfO_2, Ta_2O_5, ZrO_2 and PZT) was coated with 50 nm-thick parylene to make a hydrophobic surface and to suppress leakage of gate current. Details of the parylene-coating are described in the same reference as that for HMDS.[62] A 1000 nm-thick parylene film formed on PET was used to make a flexible FET. The thickness of the Au source/drain electrodes was 50 nm, and 3-nm thick 2,3,5,6-tetrafluoro-7,7,8,8-tetracyanoquinodimethane (F_4TCNQ) was inserted into the space between the Au electrodes and the thin film to reduce the contact resistance. The effectiveness of F_4TCNQ on a lowering of contact resistance was reported for [7]phenacene single-crystal FET in our previous article.[63] As seen from the article, large concave behaviour without F_4TCNQ was observed for the output curves in the low $|V_D|$ regime. We must stress that the insertion of F_4TCNQ is absolutely required to reduce contact resistance in phenacene single-crystal FETs. Therefore, F_4TCNQ has been inserted even for the thin-film FETs in our recent studies.[46,47]

The device structure of C_{12}-PDT thin-film FET with high-*k* gate dielectric is shown in Fig. S1 of the Electronic

Supplementary Information for easy understanding of actual FET device. The measurement system is also shown in Fig. S1. The capacitance per area, C_o, of gate dielectrics was measured using a precision LCR meter (Agilent E4980A), showing that the C_o values for SiO_2, HfO_2, Ta_2O_5, ZrO_2, PZT and parylene were 8.3 nF cm^{-2}, 35 nF cm^{-2}, 54 nF cm^{-2}, 35 nF cm^{-2}, 36 nF cm^{-2} and 3.8 nF cm^{-2}, respectively. Here, the C_o values were determined by extrapolation of the capacitances measured at 20 Hz - 1 kHz to 0 Hz. The plots of capacitance–frequency for gate dielectrics used in this study are shown in the Supplementary Information of our article.[46]

The length L of each device is indicated in the text. The channel width W was fixed at 500 μm for the FETs with SiO_2 and parylene gate dielectrics, and 600 μm for those with high-k gate dielectrics. The μ values were determined from the forward transfer curves in the saturation regime using the general MOS formula.[64] The FET characteristics were recorded using a semiconductor parameter analyser (Agilent B1500A) in an Ar-filled glove box. The source electrode was grounded (V_S = 0). Negative voltage was applied to gate and drain electrodes in measurements of transfer and output curves.

Results and discussion

Topological features of C_n-PDT thin films

Out-of-plane X-ray diffraction (XRD) patterns of the thin films of C_n-PDTs formed by thermal deposition are shown in Fig. 2. The average d_{001}, $<d_{001}>$, and the average crystallite size, $<l>$, evaluated from four reflections (001, 002, 003 and 004) are also listed in Table 1. The $<d_{001}>$ increases monotonically from 2.51(2) to 3.65(8) nm with increasing n, as seen from Table 1. The $<d_{001}>$ is plotted as a function of n (Fig. 3(a)), showing a linear relationship. The results establish that the C_n-PDTs are accurately characterised. The inclination angle, θ, with respect to c* is constant in all C_n-PDTs. Here, θ is evaluated by considering the $<d_{001}>$ and the calculated molecular lengths, yielding a value for θ of ~50º, as listed in Table 1. This θ is larger than those of phenacene molecules (20 - 30º).[43,44,47,51] A schematic representation of inclined C_{12}-PDT with respect to c* is shown in Fig. 3(b).

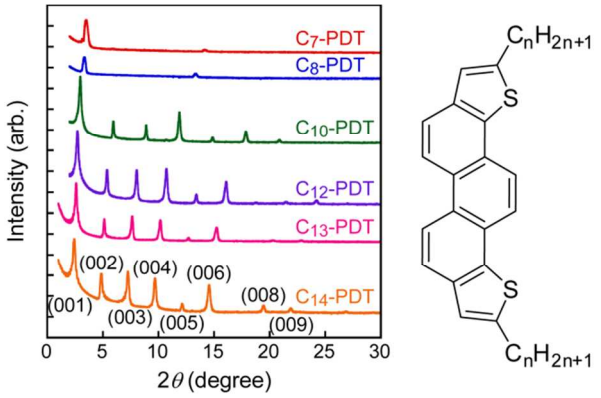

Fig. 2. XRD patterns of C_n-PDT thin films on Si/SiO_2 substrate. The molecular structure of C_n-PDT is shown. Throughout this paper, PDT-$(C_nH_{2n+1})_2$ is written as 'C_n-PDT'.

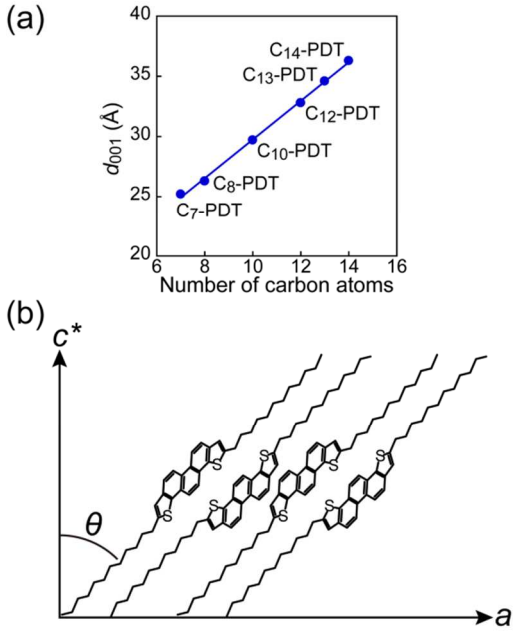

Fig. 3. (a) $<d_{001}>$ as a function of carbon atoms. (b) Schematic representation of stacking of C_n-PDT molecules

Furthermore, the crystallite size, $<l>$, of the thin films was evaluated from the full width at half maximum (FWHM) with the Debye-Scherrer formula. The maximum $<l>$ is 76(7) nm for C_{10}-PDT, while the minimum $<l>$ is 28(9) nm for C_7-PDT. The $<l>$ is the same order in all C_n-PDT thin films, but the $<l>$'s of C_7-PTD and C_8-PDT thin films are smaller than those (60 – 76 nm) of other C_n-PDT thin films. The $<l>$'s of C_{10}-PDT, C_{12}-PDT, C_{13}-PDT and C_{14}-PDT thin films are larger than those of phenacenes (35(5) nm for picene,[65] 56(8) nm for [6]phenacene,[44] 16.8(3) nm for [8]phenacene[47] and 25 nm for picene-$(C_{14}H_{29})_2$),[46] while those of C_7-PDT and C_8-PDT thin films are almost the same as those of phenacenes, as described above. As described later, the correlation between μ and $<l>$ is not so clear. In fact, the crystallite size of the C_{12}-PDT thin-film FET providing the highest $<\mu>$ value is the same as that of C_{10}-PDT, C_{13}-PDT, and C_{14}-PDT thin-film FETs. Furthermore, the XRD patterns of C_{10}-PDT, C_{12}-PDT, C_{13}-PDT, and C_{14}-PDT thin films are almost the same, exhibiting only *00l* reflections. This means that the *ab*-plane is parallel to the SiO_2 gate dielectric. By analogy with the phenacene molecules that have large transfer integrals between molecules in the *ab*-plane,[66] the conduction path of C_n-PDTs should be formed in the *ab*-plane. Therefore, these types of thin films are suitable for FET devices, in the same way as phenacene in thin-film FETs. Thin films of C_7-PDT and C_8-PDT exhibited fewer and weaker XRD peaks than other thin films, which is consistent with their smaller crystallite size. Considering only the thin films' quality, we suggest that the C_7-PDT and C_8-PDT thin-film FETs may

provide lower performance than FETs with other dialkyl-substituted PDTs.

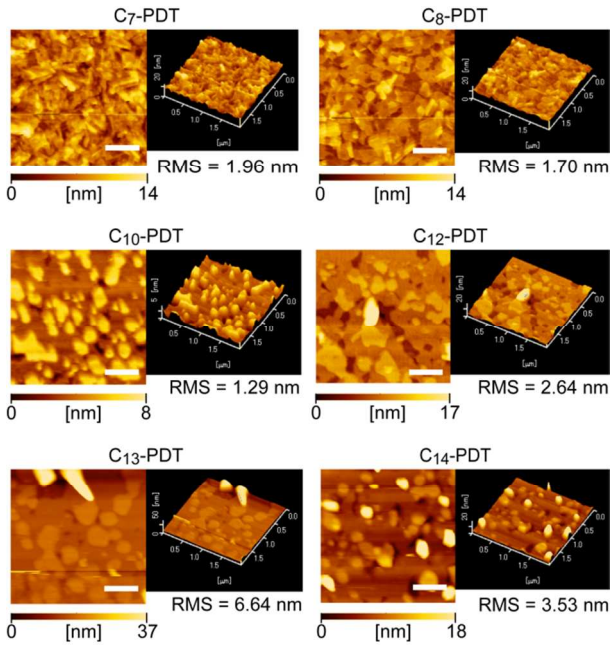

Fig. 4. AFM images of C_n-PDT thin films on Si/SiO_2 substrate. All scale bars are 500 nm.

Table 1 Morphology parameters of C_n-PDT thin films determined from XRD

n	$\langle d_{001} \rangle$ (nm)	molecular length (nm)[a]	θ (°) [b]	$\langle l \rangle$ (nm)[c]
7	2.51(2)	3.02	56	28(9)
8	2.65(1)	3.29	54	35(5)
10	2.98(4)	3.80	51	76(7)
12	3.28(2)	4.32	49	71(4)
13	3.45(4)	4.55	49	68(9)
14	3.65(8)	4.83	49	60(3)

[a] Defined as distance between the terminal methyl groups in the alkyl groups in DFT (B3LYP/6-31G (d)-optimized molecular structures. [b] Based on $\langle d_{001} \rangle$ and the molecular length. [c] From the full width at half-maximum (FWHM) of four diffraction peaks (001, 002, 003, and 004) with the Debye-Scherrer formula.

Fig. 4 shows AFM images of the thin films of C_n-PDTs. The average grain size, $\langle g \rangle$ and root-mean-square surface roughness, rms, were evaluated from the AFM images, and they are listed in Table 2. The $\langle g \rangle$ for the C_{12}-PDT thin film is the largest among these C_n-PDT thin films, showing the extended grains. However, the $\langle g \rangle$ of the C_{12}-PDT thin film is smaller than that (540 nm) of a picene thin film,[66] and the rms surface roughness of the C_{12}-PDT thin film is smaller than picene's rms (3.1 nm).[65] Judging from the difference between $\langle g \rangle$ of 300 nm and $\langle l \rangle$ of 71 nm in C_{12}-PDT thin film, a grain observed by AFM consisted of ~10^2 crystallites. From the $\langle g \rangle$ determined from the AFM images, the C_7-PDT and C_8-PDT thin films have smaller grains than other C_n-PDT thin films, which is consistent with the results determined from XRD. We assume that the C_7-PDT and C_8-PDT thin films may not provide high FET performance, but it is a little hard to predict which material's thin film among the C_{10}-PDT to C_{14}-PDT FETs provides the best FET performance.

Table 2 Morphology parameters and electronic structures of C_n-PDT thin films

n	$\langle g \rangle$ (nm)[a]	rms (nm)[a]	E_{HOMO} (eV)[a]	E_g (eV)[a]
7	$1.5(5) \times 10^2$	1.96	−5.86	3.1
8	$1.2(4) \times 10^2$	1.70	−5.85	3.1
10	$1.9(8) \times 10^2$	1.29	−5.89	3.1
12	$3(1) \times 10^2$	2.64	−5.82	3.1
13	$2.3(7) \times 10^2$	6.64	−5.82	3.1
14	$2.1(5) \times 10^2$	3.53	−5.83	3.1

[a] The parameters of morphology and electronic structure are determined from AFM and PYS / optical absorption, respectively.

Electronic features of C_n-PDT thin films

Figs. 5(a) and (b) show the PYS and optical absorption spectra of C_n-PDT thin films, respectively. The onset of the PYS spectrum can provide the energy of the HOMO level (E_{HOMO}). As seen from Fig. 5(a), the onset energy is almost the same in all C_n-PDT thin films (–5.8 ~ –5.9 eV). The E_{HOMO}'s evaluated from the PYS spectra are listed in Table 2. The E_{HOMO}'s for all C_n-PDT thin films are a little deeper than those of the corresponding phenacene molecules (–5.53 eV for picene,[41] –5.5 eV for [6]phenacene,[44,67] 5.7 eV for [7]phenacene[43]). The fact that the E_{HOMO}'s of C_n-PDT thin-films are close to each other implies that the HOMO level's wavefunction is localized in the PDT framework, an implication supported by theoretical calculations, (see Fig. 5(c) for C_{12}-PDT).

However, as seen from Fig. 6, the character of the HOMO level wavefunctions is different from those of the HOMOs in picene and picene-$(C_{14}H_{29})_2$, and it is similar to those of the HOMO-1's in picene and picene-$(C_{14}H_{29})_2$, providing a different transfer integral in the valence band between C_{12}-PDT and picene-$(C_{14}H_{29})_2$. This fact arises again when discussing the FET characteristics. The energy difference between the HOMO and HOMO-1 is very small (0.3 eV for picene, 0.1 eV for C_{12}-PDT, and 0.2 eV for picene-$(C_{14}H_{29})_2$), and the character of the HOMO wavefunction seems sensitive to small perturbations in the molecule. The E_g's of all C_n-PDT thin films were determined from the onset of their optical absorption spectra. The E_g was 3.1 eV for all C_n-PDT thin films (Fig. 5(b)). Thus, the difference in n is not reflected in the E_g. The large E_g and deep HOMO level of C_n-PDTs imply that this type of molecule is chemically stable, as are phenacene molecules.

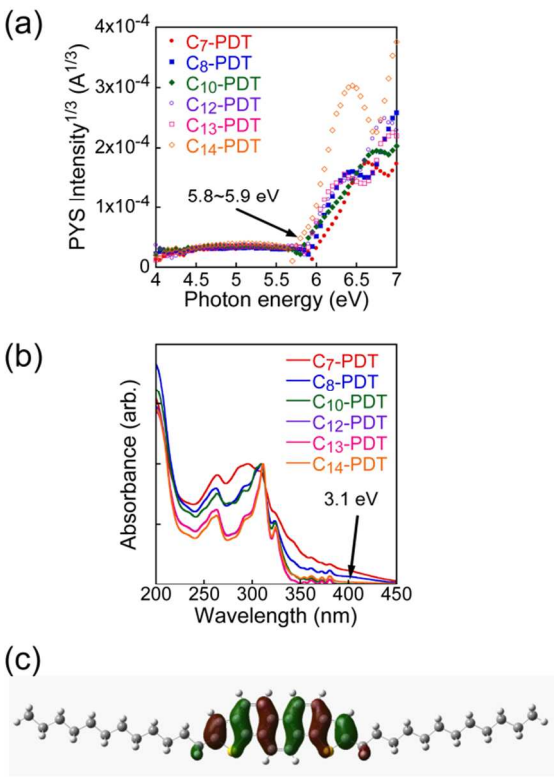

Fig. 5. (a) PYS and (b) optical absorption spectra of C_n-PDT thin films, and (c) the calculated HOMO's wavefunction for C_{12}-PDT. The PYS intensity recorded as electric current is proportional to the photoelectron yield emitted from the materials. In the case of organic semiconductors, the ionization potential (I_p) can be estimated from the 1/3rd power of PYS intensity. $E_{HOMO} = -I_p$.

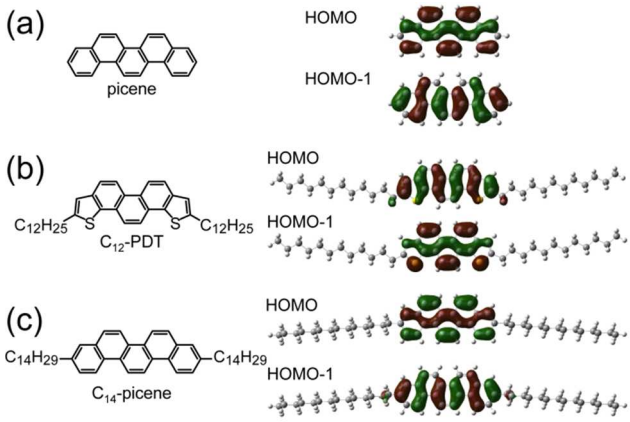

Fig. 6. The calculated wavefunctions of the HOMO and HOMO-1 of (a) picene, (b) C_{12}-PDT and (c) picene-($C_{14}H_{29}$))$_2$

FET characteristics of C_n-PDT thin-film FETs with SiO_2 gate dielectrics

As typical FET characteristics of C_n-PDTs, the transfer and output curves of a C_{12}-PDT thin-film FET with an SiO_2 gate dielectric are shown in Figs. 7(a) and (b). The L and W in this FET device are 450 and 500 μm, respectively. These curves show typical p-channel FET characteristics, in which the absolute drain current, $|I_D|$, is enhanced by applying a negative gate voltage (V_G) at the fixed drain voltage (V_D) of –120 V. Hysteresis between the forward and reverse transfer curves can be seen in Fig. 7(a). The μ values, absolute threshold voltage ($|V_{th}|$), on-off ratio, and subthreshold slope (S) were determined to be 1.4 cm^2 V^{-1} s^{-1}, 47 V, 1.0 × 10^7, and 2.4 V decade^{-1}, respectively, from the forward transfer curve shown in Fig. 7(a).

Furthermore, the values of average μ, $\langle\mu\rangle$, and the average $|V_{th}|$, $\langle|V_{th}|\rangle$, in the C_{12}-PDT thin-film FET were evaluated to be 1.1(5) cm^2 V^{-1} s^{-1} and 6(1) × 10^1 V, respectively, from nine devices; the FET parameters for nine FETs are listed in Table S1. The L was fixed at 450 μm. As seen from Table S1, the highest μ value recorded in nine FET devices reached 1.75 cm^2 V^{-1} s^{-1}. This indicates that C_{12}-PDT is a suitable organic material for the active layer of an FET device.

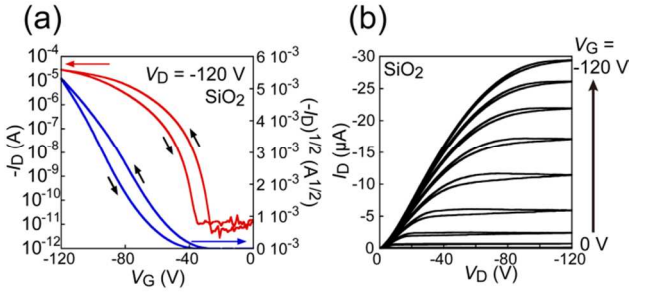

Fig. 7. (a) Transfer and (b) output curves of C_{12}-PDT thin-film FET with an SiO_2 gate dielectric

The $\langle\mu\rangle$ is higher than that of the parent PDT (1.1 × 10^{-1} cm^2 V^{-1} s^{-1}).[45] Thus, the introduction of two $C_{12}H_{29}$ chains on the PDT core improved FET characteristics. The output curve (Fig. 7(b)) of C_{12}-PDT showed linear behaviour in the low $|V_D|$ regime and saturation behaviour in the high $|V_D|$ regime; exactly saying, small concave behaviour was observed in the low $|V_D|$ regime. Therefore, the Schottky-barrier height or hole-injection barrier between thin-film and source/drain electrodes is not vanishing but small. This may be due to the insertion of F_4TCNQ, which is briefly discussed later. Thus, good FET characteristics are also shown by the output curves.

We next measured the FET characteristics of C_{12}-PDT FETs with different L's (Fig. 8). The $\langle\mu\rangle$ value is plotted as a function of L; the $\langle\mu\rangle$ was evaluated from at least three FETs. As seen from Fig. 8(a), the $\langle\mu\rangle$ increases monotonically with an increase in L, reaching a maximum at L = 450 μm, implying that the contact resistance between electrodes and thin-film affects the device's performance, *i.e.*, the contact resistance dominates the device performance at small L. Therefore, the linear behaviour in the low $|V_D|$ regime, showing small contact resistance in the output curve (Fig. 7(b)), would be produced not only by the insertion of F_4TCNQ but also by the adoption of a large L (~ 450 μm). Throughout this paper, an L of 450 μm is used in most FETs.

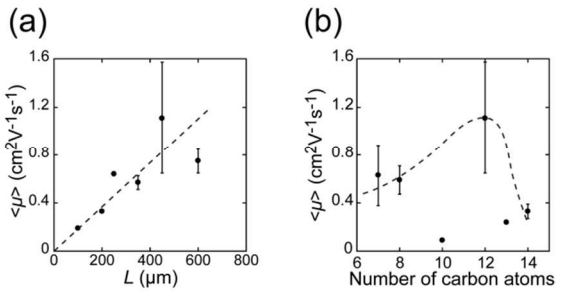

Fig. 8. (a) L dependence of <μ> in C_{12}-PDT (b) dependence of <μ> on number of C atoms (n) in each alkyl chain of C_n-PDT

The FET characteristics of all C_n-PDT thin-film FETs with an SiO_2 gate dielectric (L = 450 μm) were measured, and the μ and $|V_{th}|$ values were evaluated. All transfer and output curves of C_n-PDT thin-film FETs show typical p-channel normally-off type FET characteristics. The <μ>'s of C_n-PDT thin-film FETs are listed for n = 7 - 14 in Table 3, and the <μ> is plotted in Fig. 8(b). The average values of FET characteristics were evaluated from 3, 2, 9, 2 and 2 devices, respectively, for C_7-PDT, C_8-PDT, C_{12}-PDT, C_{13}-PDT and C_{14}-PDT thin-film FETs. The average values are not shown for the C_{10}-PDT thin-film FET because only one device was operated. Judging from the topological features of each thin film listed in Tables 1 and 2, the fact that the C_{12}-PDT gives the best FET performance among C_n-PDTs is reasonable. Namely the high crystallinity of thin film is expected for C_{12}-PDT since grain size of C_{12}-PDT thin-film is highest and <I> is also large. This must provide the high FET-performance.[68] The plot (Fig. 8(b)) shows that <μ> has no clear correlation with n (the number of carbon atoms in alkyl chains). Only the C_{12}-PDT thin-film FET showed a high <μ> (= 1.1(5) $cm^2\ V^{-1}\ s^{-1}$). The <μ> value recorded for the C_{12}-PDT thin-film FET is relatively high in organic thin-film FETs.

Recently we reported a very high μ value in a picene-$(C_{14}H_{29})_2$ thin-film FET (the highest μ = 20.6 $cm^2\ V^{-1}\ s^{-1}$ and <μ> = 14(4) $cm^2\ V^{-1}\ s^{-1}$);[46] picene-$(C_{14}H_{29})_2$ contains two alkyl chains of 14 carbon atoms. The <μ> of 1.1(5) $cm^2\ V^{-1}\ s^{-1}$ in the C_{12}-PDT thin-film FET is lower by one order of magnitude than that (14(4) $cm^2\ V^{-1}\ s^{-1}$) in the picene-$(C_{14}H_{29})_2$ thin-film FET,[46] in which the π-framework consisted of only carbon atoms, showing that a framework consisting solely of benzene rings (picene) yields better FET performance than one containing thiophene rings (PDT). This result is contrary to our expectations based on our optimistic prediction that a molecule containing thiophene rings might produce increased π-π interaction. The reason may be that the HOMO level's character is different from that of picene-$(C_{14}H_{29})_2$, *i.e.*, the HOMO's character is similar to the HOMO-1 of picene-$(C_{14}H_{29})_2$, as described above (see Fig. 6). This would clearly change the transfer integral to significantly affect the transport properties. In other words, that the valence band of C_{12}-PDT has a HOMO different from that of picene-$(C_{14}H_{29})_2$ may be the origin of the lower FET properties. This implies that we may pursue higher FET properties by suppressing the switching of HOMO and HOMO-1 in phenacene-type molecules containing thiophene rings. A specific material design will be suggested in the final part of this paper. Furthermore, the fact that the best FET performance was observed in C_{12}-PDT (12 carbon atoms in the alkyl chains) among the C_n-PDTs is unlike what was observed in picene-$(C_{14}H_{29})_2$ (14 carbon atoms). Namely, the number of carbon atoms in alkyl chains suitable for the active layer in FET is specific to each molecule.

Table 3 FET characteristics of C_n-PDT FETs: L = 450 μm.

N	<μ> ($cm^2\ V^{-1}\ s^{-1}$)	<$\lvert V_{th}\rvert$> (V)	<$I_{on/off}$>	<S> (V decade^{-1})
7	$4(3) \times 10^{-1}$	$7(2) \times 10^{1}$	$5(5) \times 10^{5}$	5(2)
8	$6(1) \times 10^{-1}$	$4.8(9) \times 10^{1}$	$7(2) \times 10^{5}$	5.5(4)
10	9×10^{-2}	6×10^{1}	7×10^{4}	2.4
12	1.1(5)	$6(1) \times 10^{1}$	$4(7) \times 10^{6}$	6(4)
13	$2.39(2) \times 10^{-1}$	$4.8(2) \times 10^{1}$	$2(2) \times 10^{6}$	1.4(2)
14	$3.3(6) \times 10^{-1}$	$5(2) \times 10^{1}$	$2(2) \times 10^{6}$	2.5(4)

FET characteristics of C_{12}-PDT thin-film FETs with high-k gate dielectrics

The transfer and output curves of a C_{12}-PDT thin-film FET with a PZT gate dielectric (L = 450 μm) are shown in Figs. 9(a) and (b). These curves also show p-channel FET characteristics. The curves in Fig. 9 show low-voltage operation in this FET device, which operates at $|V_D|$ = 20 V. As the C_o of PZT is 36 nF cm^{-2}, low-voltage operation is reasonable. The μ, $|V_{th}|$, on-off ratio, and S factors were evaluated to be 6.4×10^{-1} $cm^2\ V^{-1}\ s^{-1}$, 8.7 V, 1.7×10^5, and 8.3×10^{-1} V decade^{-1}, respectively, showing low-voltage operation ($|V_{th}|$ = 8.7 V). The output characteristics show linear (low $|V_D|$ regime) and saturation behaviour (high $|V_D|$ regime); in Fig. 9(b), small concavity is observed in low $|V_D|$ regime, showing small contact resistance. The values of <μ> and <$|V_{th}|$> in the C_{12}-PDT thin-film FET (L = 450 μm) were found to be 6.5(7) × 10^{-1} $cm^2\ V^{-1}\ s^{-1}$ and 8(1) V, respectively, from 3 FET devices, which are listed in Table S2 of the Electronic Supplementary Information. Furthermore, we fabricated C_{12}-PDT FET devices with HfO_2, Ta_2O_5 and ZrO_2 gate dielectrics (L = 450 μm). As seen from Table S2, the values of <μ> and $|V_{th}|$ are 1.7(6) $cm^2\ V^{-1}\ s^{-1}$ and 11.6(6) V, respectively, for the HfO_2 gate dielectric, $7(2) \times 10^{-1}$ $cm^2\ V^{-1}\ s^{-1}$ and 11.5(7) V, respectively, for the Ta_2O_5 gate dielectric, and 1.8(6) $cm^2\ V^{-1}\ s^{-1}$ and 11.9(2) V, respectively, for the ZrO_2 gate dielectric; the FET characteristics of the C_{12}-PDT thin-film FET with ZrO_2 gate dielectric are shown in Figs. 9(c) and (d). Thus, <μ> values higher than 1 $cm^2\ V^{-1}\ s^{-1}$ were recorded with HfO_2 and ZrO_2. Low-voltage operation was simultaneously realized using high-k gate dielectrics. We regard the C_{12}-PDT thin-film FETs exhibiting the above <μ> values as promising organic FETs. Although the performance of FETs with C_{12}-PDT

molecules is still lower than that of dialkyl-substituted picenes, the field-effect mobility and operation voltage achieved in this study show the potential usefulness of these types of molecules in FET devices.

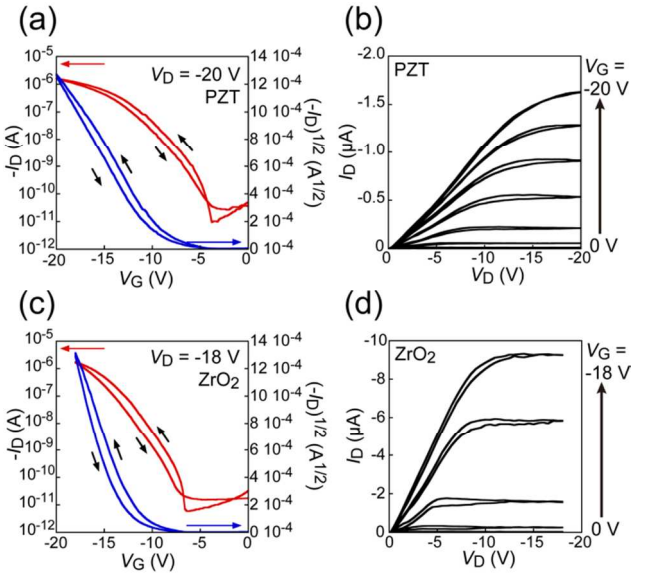

Fig. 9. (a) Transfer and (b) output curves of C_{12}-PDT thin-film FET with a PZT gate dielectric (c) Transfer and (d) output curves of C_{12}-PDT thin-film FET with a ZrO_2 gate dielectric

Fabrication of flexible C_{12}-PDT thin-film FET with a parylene gate dielectric formed on a PET substrate

We tried to fabricate a flexible FET using thin films of C_{12}-PDT (L = 135, 200 and 300 mm) and a parylene gate dielectric formed on a polyethylene terephthalate (PET) substrate. As described later, the μ value in this C_{12}-PDT thin-film FET with parylene / PET substrate was independent of L. The transfer and output curves are shown in Figs. 10(a) and (b) (L = 135 μm). The μ and $|V_{th}|$ were 2.2 × 10^{-2} cm^2 V^{-1} s^{-1} and 94 V, respectively. The $<\mu>$ and $<|V_{th}|>$ were found to be 2.1(5) × 10^{-2} cm^2 V^{-1} s^{-1} and 1.1(1) × 10^2 V, respectively, from three FET devices. A photograph of the flexible FET device is shown in Fig. 10(c); this device can be bent easily. The FET performance is still lower by two orders of magnitude than that in C_{12}-PDT thin-film FETs with SiO_2 and high-k gate dielectrics. This reason is unclear, but the parylene on PET may not be so flat. This may lead to the lowering of performance. The improvement of FET performance in the flexible FET is the next important research-subject. Nevertheless, this success in observing FET characteristics in a C_{12}-PDT thin-film FET with a parylene / PET substrate opens a path to future practical FET devices that are both flexible and light in weight.

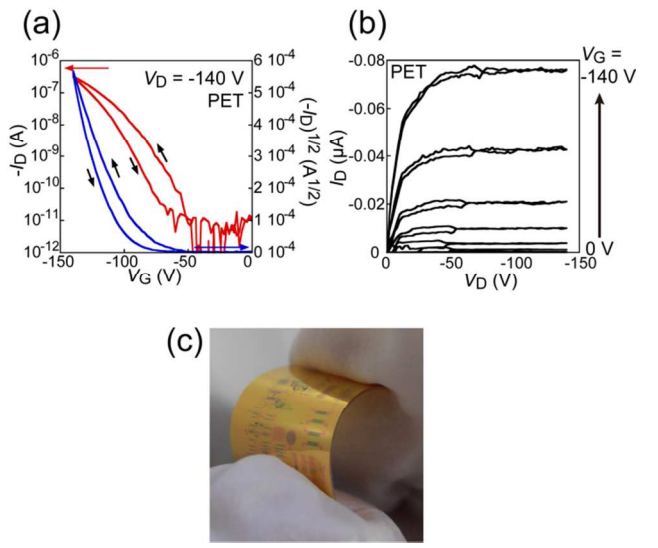

Fig. 10. (a) Transfer and (b) Output curves of C_{12}-PDT thin-film FET with a parylene gate dielectric (c) A photograph of the FET being flexed between fingers.

Conclusions

We have demonstrated the use of a new class of 2,9-dialkylated PDT derivatives in thin-film FET devices. High-performance FET characteristics have been observed in C_{12}-PDT thin-film FETs. The highest μ value reached 2.2 cm^2 V^{-1} s^{-1} in a C_{12}-PDT thin-film FET with a HfO_2 gate dielectric; an average value of μ as high as 1.8(6) cm^2 V^{-1} s^{-1} was observed in a C_{12}-PDT thin-film FET with a ZrO_2 gate dielectric. Low-voltage operation ($<|V_{th}|>$ ~ 11 V) was also achieved, which implies that C_{12}-PDT is a promising material for FET application. In this study, we have also succeeded in operating a flexible C_{12}-PDT thin-film FET. As predicted from topological characterizations (XRD and AFM), the C_7-PDT and C_8-PDT thin-film FETs did not show high FET performance. However, the topological characterizations could not reliably predict the most promising material among the C_n-PDTs tested. The FET characterizations achieved in this study showed a significant difference among C_n-PDTs. A phenacene-type molecule (C_{12}-PDT) containing thiophene rings could produce a high-performance FET with a $<\mu>$ higher than 1 cm^2 V^{-1} s^{-1}, but the performance of the C_{12}-PDT thin-film FET was still lower by one order of magnitude than a picene-$(C_{14}H_{29})_2$ thin-film FET ($<\mu>$ = 14(4) cm^2 V^{-1} s^{-1}).[38] For this reason, we suggested that the switching of HOMO and HOMO-1 occurred between picene/picene-$(C_{14}H_{29})_2$ and C_{12}-PDT may be a key. Furthermore, we remarked the larger inclined angle (θ = 50º) which may lead to the smaller transfer integral because of smaller π-π overlapping between molecules. The relationship between θ and μ may be an interesting problem to be pursued. To sum up, this study convinced us that a phenacene-type molecule can serve as the basis for practical FETs.

Here, we give a comment on solution-processed FET with C_{12}-PDT, because one purpose of alkyl-substitution is absolutely to fabricate high-performance FET by a solution-

process. The solution-processed C_{12}-PDT thin-film FET was preliminary fabricated using an SiO_2 gate dielectric. Its device structure and the transfer/output curves are shown in the Electronic Supplementary Information. Because of low-quality of thin-film prepared by a solution process (grains aggregate), the μ value was still 10^{-2} cm^2 V^{-1} s^{-1}. The optimization of solution-processed film is indispensable for realization of high-performance FETs.

Finally, we need to show a strategy to synthesize new phenacene-type materials that can provide more practical high-performance FETs. The C_n-PDT thin-film FETs could not exceed the maximum μ value (= 20.9 cm^2 V^{-1} s^{-1}) or $<\mu>$ (= 14(4) cm^2 V^{-1} s^{-1}) recorded for picene-$(C_{14}H_{29})_2$ thin-film FETs. As we have already suggested in this paper, the fact that the HOMO level's character is different from that of picene-$(C_{14}H_{29})_2$ may explain the observation of lower FET properties. Therefore, we must design new molecules with HOMO characteristics similar to those of picene-$(C_{14}H_{29})_2$. One idea is to introduce the thiophene rings not to the ends of the picene molecules but to the inner part, which may produce similar HOMO characteristics to picene-$(C_{14}H_{29})_2$, as suggested by the recent study on picene and dinaphtho[1,2-*b*:2',1'-*d*]chalcogenophenes by Mitsui *et al*.[69] Thus, this study may have provided another clue to guide the search for new materials to construct even higher performance FETs.

Acknowledgements

This study was partly supported by Grants-in-aid (22244045, 24654105, and 23684028) from MEXT, the Strategic International Collaborative Research Program (JST/SICORP, EU-JPN LEMSUPER), and the Program for Promoting the Enhancement of Research Universities from MEXT and a Special Project of Okayama University. We gratefully thank Ms. Megumi Kosaka and Mr. Motonari Kobayashi at the Department of Instrumental Analysis, Advanced Science Research Center, Okayama University, for the elemental analyses, and the SC-NMR Laboratory of Okayama University for the NMR spectral measurements.

Notes and references

[a] Research Laboratory for Surface Science, Okayama University, Okayama 700-8530, Japan

[b] Research Center of New Functional Materials for Energy Production, Storage and Transport, Okayama University, Okayama 700-8530, Japan

[c] Japan Science and Technology Agency, ACT-C, 4-1-8 Honcho, Kawaguchi, Saitama 332-0012, Japan

[d] Division of Earth, Life, and Molecular Sciences, Graduate School of Natural Science and Technology, Okayama University, 3-1-1 Tsushimanaka, Kita-ku, Okayama 700-8530, Japan

† Electronic Supplementary Information (ESI) available. See DOI: 10.1039/c000000x/

1. Y. Sun, Y. Liu and D. Zhu, *J. Mater. Chem*., 2005, **15**, 53−65.
2. A. R. Murphy and J. M. Fréchet, *Chem. Rev*., 2007, **107**, 1066−1096.
3. J. E. Anthony, *Angew. Chem., Int. Ed. Engl.*, 2008, **47**, 452−483.
4. S. Allard, M. Forster, B. Souharce, H. Thiem and U. Scherf, *Angew. Chem., Int. Ed. Engl.*, 2008, **47**, 4070−4098.
5. Y. Yamashita, *Sci. Technol. Adv. Mater*., 2009, **10**, 024313.
6. H. Klauk, M. Halik, U. Zschieschang, F. Eder, G. Schmid and C. Dehm, *Appl. Phys. Lett*., 2003, **82**, 4175–4177.
7. K. Takimiya, H. Ebata, K. Sakamoto, T. Izawa, T. Otsubo and Y. Kunugi, *J. Am. Chem. Soc*., 2006, **128**, 12604−12605.
8. H. Ebata, T. Izawa, E. Miyazaki, K. Takimiya, M. Ikeda, H. Kuwabara and T. Yui, *J. Am. Chem. Soc*., 2007, **129**, 15732−15733.
9. T. Yamamoto and K. Takimiya, *J. Am. Chem. Soc*., 2007, **129**, 2224−2225.
10. C. D. Sheraw, T. N. Jackson, D. L. Eaton and J. E. Anthony, *Adv. Mater*., 2003, **15**, 2009−2011.
11. M. P. Payne, S. R. Parkin, J. E. Anthony, C.-C. Kuo and T. N. Jackson, *J. Am. Chem. Soc*., 2005, **127**, 4986−4987.
12. T. Mori, T. Nishimura, T. Yamamoto, I. Doi, E. Miyazaki, I. Osaka, and K. Takimiya, *J. Am. Chem. Soc*., 2013, **135**, 13900−13913.
13. C. Mitsui, T. Okamoto, M. Yamagishi, J. Tsurumi, K. Yoshimoto, K. Nakahara, J. Soeda, Y. Hirose, H. Sato, A. Yamano, T. Uemura, and J. Takeya, *Adv. Mater.*, 2014, **26**, 4546−4551.
14. H. Meng, F. Sun, M. B. Goldfinger, G. D. Jaycox, Z. Li, W. J. Marshall and G. S. Blackman, *J. Am. Chem. Soc.*, 2005, **127**, 2406−2407.
15. H. Klauk, U. Zschieschang, R. T. Weitz, H. Meng, F. Sun, G. Nunes, D. E. Keys, C. R. Fincher and Z. Xiang, *Adv. Mater*., 2007, **19**, 3882−3887.
16. M. Halik, H. Klauk, U. Zschiesshang, G. Schmid, S. Ponomarenko, S. Kirchmeyer and W. Weber, *Adv. Mater*., 2003, **15**, 917−922.
17. M. Takada, H. Graaf, Y. Yamashita and H. Tada, *Japan J. Appl. Phys*., 2002, **41**, L4−L6.
18. Naraso, J. Nishida, S. Ando, J. Yamaguchi, K. Itaka, H. Koinuma, H. Tada, S. Tokito and Y. Yamashita, *J. Am. Chem. Soc*., 2005, **127**, 10142−10143.
19. P. R. L. Malenfant, C. D. Dimitrakopoulos, J. D. Gelorme, L. L. Kosbar, T. O. Graham, A. Curioni and W. Andreoni, *Appl. Phys. Lett*., 2002, **80**, 2517−2519.
20. B. A. Jones, M. J. Ahrens, M.-H. Yoon, A. Facchetti, T. J. Marks and M. R. Wasielewski, *Angew. Chem., Int. Ed. Engl.*, 2004, **43**, 6363−6366.
21. J. H. Oh, S.-L. Suraru, W.-Y. Lee, M. Köenemann, H. W. Höffken, C. Roeger, R. Schmidt, Y. Chung, W.-C. Chen, F. Würthner, and Z. Bao, *Adv. Funct. Mater*., 2010, **20**, 2148−2156.
22. F. Zhang, Y. Hu, T. Schuettfort, C.-a. Di, X. Gao, C. R. McNeill, L. Thomsen, S. C. B. Mannsfeld, W. Yuan, H. Sirringhaus, and D. Zhu, *J. Am. Chem. Soc*., 2013, **135**, 2338-2349.
23. S. Kobayashi, T. Takenobu, S. Mori, A. Fujiwara and Y. Iwasa, *Appl. Phys. Lett*., 2003, **82**, 4581−4583.
24. P. H. Wöbkenberg, J. Ball, D. D. C. Bradley, T. D. Anthopoulos, F. Kooistra, J. C. Hummelen and D. M. Leeuw, *Appl. Phys. Lett.*, 2008, **92**, 143310.
25. J. Youn, P.-Y. Huang, Y.-W. Huang, M.-C. Chen, Y.-J. Lin, H. Huang, R. P. Ortiz, C. Stern, M.-C. Chung, L.-H. Chen, A. Facchetti, T. J. Marks, *Adv. Funct. Mater.* 2012, **22**, 48−60.
26. M. C. Chen, Y. J. Chiang, C. Kim, Y. J. Guo, S. Y. Chen, Y. J. Liang, Y. W. Huang, T. S. Hu, G. H. Lee, A. Facchetti, T. J. Marks, *Chem. Commun.* **2009**, 1846−1848.

27. Q. Wu, R. Li, W. Hong, H. Li, X. Gao, D. Zhu, *Chem. Mater.* 2011, **23**, 3138−3140.
28. V. C. Sundar, J. Zaumseil, V. Podzorov, E. Menard, R. L. Willett, T. Someya, M. E. Gershenson and J. A. Rogers, *Science*, 2004, **303**, 1644−1645.
29. J. Takeya, M. Yamagishi, Y. Tominari, R. Hirahara, Y. Nakazawa, T. Nishikawa, T. Kawase, T. Shimoda and S. Ogawa, *Appl. Phys. Lett*., 2007, **90**, 102120.
30. H. Moon, R. Zeis, E.-J. Borkent, C. Besnard, A. J. Lovinger, T. Siegrist, C. Kloc and Z. Bao, *J. Am. Chem. Soc*. 2004, **126**, 15322−15323.
31. M. Mas-Torrent, P. Hadley, S. T. Bromley, N. Crivillers, J. Veciana and C. Rovira, *Appl. Phys. Lett*., 2005, **86**, 012110.
32. M. Mas-Torrent, M. Durkut, P. Hadley, X. Ribas and C. Rovira, *J. Am. Chem. Soc*., 2004, **126**, 984−985.
33. T. Yasuda, T. Goto, K. Fujita and T. Tsutsui, *Appl. Phys. Lett*., 2004, **85**, 2098−2100.
34. B. Park, I. In, P. Gopalan, P. G. Evans, S. King and P. F. Lyman, *Appl. Phys. Lett.* 2008, **92**, 133302.
35. Z. Li , J. Du, Q. Tang, F. Wang, J. C. Yu and Q. Miao, *Adv. Mater.* 2010, **22**, 3242−3246.
36. H. M. Lee, H. Moon b, H.-S. Kim, Y. N. Kim, S.-M. Choi, S. Yoo and S. O. Cho, *Org. Electron.* 2011, **12**, 1446−1453.
37. X. Qian, T. Wang and D. Yan, *Org. Electron.* 2013, **14**, 1052−1056.
38. T. Kanashima, Y. Katsura and M. Okuyama, *Jpn. J. Appl. Phys.* 2014, **53**, 04ED11,
39. R. Mitsuhashi, Y. Suzuki, Y. Yamanari, H. Mitamura, T. Kambe, N. Ikeda, H. Okamoto, A. Fujiwara, M. Yamaji, N. Kawasaki, Y. Maniwa and Y. Kubozono, *Nature*, 2010, **464**, 76−79.
40. Y. Kubozono, H. Mitamura, X. Lee, X. He, Y. Yamanari, Y. Takahashi, Y. Suzuki, Y. Kaji, R. Eguchi, K. Akaike, T. Kambe, H. Okamoto, A. Fujiwara, T. Kato, T. Kosugi and H. Aoki, *Phys. Chem. Chem. Phys.*, 2011, **13**, 16476−16493.
41. H. Okamoto, N. Kawasaki, Y. Kaji, Y. Kubozono, A. Fujiwara and M. Yamaji, *J. Am. Chem. Soc*., 2008, **130**, 10470−10471.
42. N. Kawasaki, Y. Kubozono, H. Okamoto, A. Fujiwara and M. Yamaji, *Appl. Phys. Lett*., 2009, **94**, 043310.
43. Y. Sugawara, Y. Kaji, K. Ogawa, R. Eguchi, S. Oikawa, H. Gohda, A. Fujiwara and Y. Kubozono, *Appl. Phys. Lett*., 2011, **98**, 013303.
44. N. Komura, H. Goto, X. He, H. Mitamura, R. Eguchi, Y. Kaji, H. Okamoto, Y. Sugawara, S. Gohda, K. Sato and Y. Kubozono, *Appl. Phys. Lett.*, 2012, **101**, 083301.
45. R. Eguchi, X. He, S. Hamao, H. Goto, H. Okamoto, S. Gohda, K. Sato and Y. Kubozono, *Phys. Chem. Chem. Phys*., 2013, **15**, 20611−20617.
46. H. Okamoto, S. Hamao, H. Goto, Y. Sakai, M. Izumi, S. Gohda, Y. Kubozono and R. Eguchi, *Sci. Rep*., 2014, **4**, 5048.
47. H. Okamoto, R. Eguchi, S. Hamao, H. Goto, K. Gotoh, Y. Sakai, M. Izumi, Y. Takaguchi, S. Gohda and Y. Kubozono, *Sci. Rep.*, 2014, **4**, 5330.
48. Y. Yuan, G. Giri, A. L. Ayzner, A. P. Zoombelt, S. C. B. Mannsfeld, J. Chen, D. Nordlund, M. F. Toney, J. Huang and Z. Bao, *Nat. Commun.,* 2014, **5**, 3005.
49. X. Lee, Y. Sugawara, A. Ito, S. Oikawa, N. Kawasaki, Y. Kaji, R. Mitsuhashi, H. Okamoto, A. Fujiwara, K. Omote, T. Kambe, N. Ikeda and Y. Kubozono, *Org. Electron*., 2010, **11**, 1394−1398.
50. Y. Sugawara, K. Ogawa, H. Goto, S. Oikawa, K. Akaike, N. Komura, R. Eguchi, Y. Kaji, S. Gohda and Y. Kubozono, *Sens. Actuators, B* 2012, **171 / 172**, 544−549.
51. Y. Kubozono, X. He, S. Hamao, K. Teranishi, H. Goto, R. Eguchi, T. Kambe, S. Gohda and Y. Nishihara, *Eur. J. Inorg. Chem*., **2014**, 3806−3819.
52. N.-H. Chang, X.-C. Chen, H. Nonobe, Y. Okuda, H. Mori, K. Nakajima and Y. Nishihara, *Org. Lett*., 2013, **15**, 3558−3561.
53. N.-H. Chang, H. Mori, X-C. Chen, Y. Okuda, T. Okamoto and Y. Nishihara, *Chem. Lett*., 2013, **42**, 1257−1259.
54 Y. Nishihara, M. Kinoshita, K. Hyodo, Y. Okuda, R. Eguchi, H. Goto, S. Hamao, Y. Takabayashi and Y. Kubozono, *RSC Adv.*, 2013, **3**, 19341−19347.
55 H. Inokuchi, G. Saito, P. Wu, K. Seki, T. B. Tang, T. Mori, K. Imaeda, T. Enoki, Y. Higuchi, K. Inaka, N. Yasuoka, *Chem. Lett.* **1986**, 1263−1266.
56. M. J. Kang, I. Doi, H. Mori, E. Miyazaki, K. Takimiya, M. Ikeda and H. Kuwabara, *Adv. Mater.* 2011, **23**, 1222−1225.
57. K. Hyodo, H. Nonobe, S. Nishinaga and Y. Nishihara, *Tetrahedron Lett.*, 2014, **55**, 4002−4005.
58. Gaussian 09, Revision A.02, M. J. Frisch, G. W. Trucks, H. B. Schlegel, G. E. Scuseria,M. A. Robb, J. R. Cheeseman, G. Scalmani, V. Barone, B. Mennucci, G. A. Petersson, H. Nakatsuji, M. Caricato, X. Li, H. P. Hratchian, A. F. Izmaylov, J. Bloino, G. Zheng, J. L. Sonnenberg, M. Hada, M. Ehara, K. Toyota, R. Fukuda, J. Hasegawa, M. Ishida, T. Nakajima, Y. Honda, O. Kitao, H. Nakai, T. Vreven, J. Jr. Montgomery, J. E. Peralta, F. Ogliaro, M. Bearpark, J. J. Heyd, E. Brothers, K. N. Kudin, V. N. Staroverov, R. Kobayashi, J. Normand, K. Raghavachari, A. Rendell, J. C. Burant, S. S. Iyengar, J. Tomasi, M. Cossi, N. Rega, J. M. Millam, M. Klene, J. E. Knox, J. B. Cross, V. Bakken, C. Adamo, J. Jaramillo, R. Gomperts, R. E. Stratmann, O. Yazyev, A. J. Austin, R. Cammi, C. Pomelli, J. W. Ochterski, R. L. Martin, K. Morokuma, V. G. Zakrzewski, G. A. Voth, P. Salvador, J. J. Dannenberg, S. Dapprich, A. D. Daniels, O. Farkas, J. B. Foresman, J. V. Ortiz, J. Cioslowski, D. J. Fox, Gaussian, Inc., Wallingford, CT, ***2009***.
59. A. D. Becke, *J. Chem. Phys.* 1993, **98**, 5648−5652.
60. C. Lee, W. Yang and R. G. Parr, *Phys. Rev. B.*, 1988, **37**, 785−789.
61. W. J. Hehre, L. Radom, P. V. R. Schleyer, J. Pople, *Ab Initio Molecular Orbital Theory; John Wiley: New York, NY*, **1986**.
62. N. Kawasaki, W. L. Kalb, T. Mathis, Y. Kaji, R. Mitsuhashi, H. Okamoto, Y. Sugawara, A. Fujiwara and Y. Kubozono, *Appl. Phys. Lett.*, 2010, **96**, 113305.
63. X. He, S. Hamao, R. Eguchi, H. Goto, Y. Yoshida, G. Saito and Y. Kubozono, *J. Phys. Chem. C,* 2014, **118**, 5284−5293.
64. S. M. Sze, *Semiconductor devices*, physics and technology, John Wiley & Sons. Inc., 2nd edn., New York, 1985 ch. 6, pp. 187−194.
65. Y. Kaji, N. Kawasaki, X. Lee, H. Okamoto, Y. Sugawara, S. Oikawa, A. Ito, H. Okazaki, T. Yokoya, A. Fujiwara and Y. Kubozono, *Appl. Phys. Lett.*, 2009, **95**, 183302.
66. H. Mori, X.-C. Chen, N.-H. Chang, S. Hamao, Y. Kubozono, K Nakajima and Y. Nishihara, *J. Org. Chem.*, 2014, **79**, 4973−4983.
67. X. He, R. Eguchi H. Goto, E. Uesugi, S. Hamao, Y. Takabayashi and Y. Kubozono, *Org. Electron.*, 2013, **14**, 1673−1682.
68. J. Youn, S. Kewalramani, J. D. Emery, Y. Shi, S. Zhang, H.-C. Chang, Y.-J. Liang, C.-M. Yeh, C.-Y. Feng, H. Huang, C. Stern, L.-H. Chen, J.-C. Ho , M.-C. Chen, M. J. Bedzyk, A. Facchetti, T. J. Marks , *Adv. Funct. Mater.* 2013, **23**, 3850−3865.

69. C. Mitsui, T. Okamoto, H. Matsui, M. Yamagishi, T. Matsushita, J. Soeda, K. Miwa, H. Sato, A. Yamano, T. Uemura and J. Takeya, *Chem. Mater.* 2013, **25**, 3952−3956.

Transistor application of new picene-type molecules, 2,9-dialkylated phenanthro[1,2-*b*:8,7-*b*']dithiophenes

Yoshihiro Kubozono, Keita Hyodo, Hiroki Mori, Shino Hamao, Hidenori Goto and Yasushi Nishihara

J. Mater. Chem., 2014, **xx**, xxxx-xxxx.
DOI: 10.1039/C2JMxxxxx

Field-effect transistors have been fabricated that use thin films of 2,9-dialkylated phenanthro[1,2-*b*:8,7-*b*']dithiophenes (C_n-PDTs), with the transistor based on a thin film of C_{12}-PDT showing a μ as high as ~2 cm^2 V^{-1} s^{-1}, which is promising for future practical electronics.